catalysts

MDPI

Article

A Novel Pd-P Nano-Alloy Supported on Functionalized Silica for Catalytic Aerobic Oxidation of Benzyl Alcohol

Seyed Sepehr Moeini [1,*], Umberto Pasqual Laverdura [1], Eleonora Marconi [1], Nicola Lisi [2], Emanuele Serra [2], Rosa Chierchia [2], Igor Luisetto [2], Simonetta Tuti [1] and Daniela Tofani [1]

[1] Section of Nanoscience and Nanotechnologies, Department of Science, "Roma Tre" University, Via della Vasca Navale, 79, 00146 Rome, Italy; umberto.pasquallaverdura@uniroma3.it (U.P.L.); eleonora.marconi@uniroma3.it (E.M.); simonetta.tuti@uniroma3.it (S.T.); daniela.tofani@uniroma3.it (D.T.)

[2] Italian National Agency for New Technologies, Energy and Sustainable Economic Development (ENEA), Via Anguillarese, 301, 00123 Rome, Italy; nicola.lisi@enea.it (N.L.); emanuele.serra@enea.it (E.S.); rosa.chierchia@enea.it (R.C.); igor.luisetto@enea.it (I.L.)

* Correspondence: seyedsepehr.moeini@uniroma3.it

Abstract: Catalytic aerobic oxidation of benzyl alcohol (BnOH) to benzaldehyde (PhCHO) over supported noble metal catalysts has grabbed the attention of researchers due to the critical role of PhCHO in numerous industrial syntheses. In the present study, a novel catalyst, Pd-P alloy supported on aminopropyl-functionalized mesoporous silica (NH_2-SiO_2), was prepared through in situ reduction and characterized by BET-BJH analysis, SEM, TEM, XRD, FTIR, TG-DTA, and XPS. Chemical properties and catalytic performance of Pd-P/NH_2-SiO_2 were compared with those of Pd° nanoparticles (NPs) deposited on the same support. Over Pd-P/NH_2-SiO_2, the BnOH conversion to PhCHO was much higher than over Pd°/NH_2-SiO_2, and significantly influenced by the nature of solvent, reaching 57% in toluene at 111 °C, with 63% selectivity. Using pure oxygen as an oxidant in the same conditions, the BnOH conversion increased up to 78%, with 66% selectivity. The role of phosphorous in improving the activity may consist of the strong interaction with Pd that favours metal dispersion and lowers Pd electron density.

Keywords: benzyl alcohol; functionalized silica; palladium nanoparticles; palladium-phosphorous alloy; aerobic oxidation; benzaldehyde; selectivity

Citation: Moeini, S.S.; Pasqual Laverdura, U.; Marconi, E.; Lisi, N.; Serra, E.; Chierchia, R.; Luisetto, I.; Tuti, S.; Tofani, D. A Novel Pd-P Nano-Alloy Supported on Functionalized Silica for Catalytic Aerobic Oxidation of Benzyl Alcohol. *Catalysts* **2022**, *12*, 20. https://doi.org/10.3390/catal12010020

Academic Editor: Werner Oberhauser

Received: 24 November 2021
Accepted: 22 December 2021
Published: 25 December 2021

1. Introduction

Oxidation of alcohols is amongst the most crucial and widely utilized reactions for synthesizing organic materials and developing key intermediate chemicals in petroleum and biorefinery sectors [1,2]. In particular, oxidation of benzyl alcohol (BnOH) to benzaldehyde (PhCHO) is of paramount importance, because the product is an indispensable intermediate for many organic syntheses [3], and is utilized in manufacturing pharmaceuticals and therapeutics, dyestuffs, fragrances, and flavours [4]. Traditionally, PhCHO is produced by hydrolysis of benzylidene chloride, which leaves undesirable chlorine contamination, or, by partial oxidation of toluene which suffers from low PhCHO selectivity [5,6]. On the other hand, BnOH oxidation has been mostly performed via expensive strong oxidants, mainly chromates, and permanganates, which pose serious environmental concerns. Therefore, developing catalytic systems for efficient and selective oxidation of BnOH to PhCHO with air or molecular oxygen has attracted many researchers in recent decades [7].

Numerous supported noble metal nanoparticles (NPs) such as Pt [8], Pd [9–15], Ru [16], and Au [17], have been developed and examined. Among them, Pd-based catalysts have been widely studied due to their high activity, and selectivity towards PhCHO [18,19]. The catalytic activity of such noble metal nanoparticles depends on their valence, physicochemical properties, size, and morphology. On the other hand, the size and dispersion of these nanoparticles largely depend on the properties of the support. The electronic effect and

structural binding forces between support materials and metal NPs are key factors that affect the selective oxidation reactions [1,18,20,21].

Mesoporous silica materials proved to be one of the most beneficial supports for metal NP catalysts owing to their high thermal and chemical stability, great surface area, tunable pore size, and provision of highly dispersed active sites on the final catalyst [22–24]. Catalysts manufactured by supporting palladium NPs on silica have been utilized in numerous reactions such as Suzuki coupling reactions, C—H activation [25,26], and aerobic oxidation of benzyl alcohol [27]. The mildly acidic surface of the pristine silica acts as a barrier for absorption and diffusion of the palladium and/or its precursors; therefore, functionalizing the surface of the support to increase the basicity, is deemed necessary to improve the metal deposition and to obtain smaller particle size [12,22,28,29]. For example, Chen et al., found that functionalizing SBA-16 silica with aminopropyl groups remarkably improved the catalytic activity, the BnOH conversion, and the selectivity towards PhCHO [29].

Furthermore, alloying palladium with non-metal elements such as phosphorous has been studied. Pd-P alloy has been applied as catalyst for methanol [30], and ethylene glycol oxidation [31]. Recently, Guo et al. showed that utilizing Pd-P alloy supported on a porous carbon frame (PCF) has threefold enhanced BnOH conversion and turnover frequency (TOF) with respect to simple Pd° metal deposited on the same support [10].

In the present research work, a novel catalyst, palladium–phosphorus nano-alloy supported on aminopropyl-functionalized mesoporous silica (Pd-P/NH_2-SiO_2) was synthesized and characterized. The chemical-physical properties and the catalytic performance for aerobic BnOH to PhCHO oxidation of this catalyst were examined and compared to those of Pd° supported on the same aminopropyl-functionalized mesoporous silica (Pd°/NH_2-SiO_2).

2. Results and Discussion

2.1. Synthesis of Catalysts

In the initial catalyst preparations, loading Pd° or Pd-P alloy on pristine mesoporous silica was unsuccessful, using the same procedures, respectively described in Sections 3.1.4 and 3.1.5. At the end of the procedures, two visually distinguishable phases of metal and support were formed in the centrifuge tubes (Figure S1, Supplementary Materials). However, such an outcome was not unexpected because, in general, palladium and other noble metals are not easily absorbed in the silica [12,22].

Therefore, aiming at improving the metal deposition process and strengthening the support/metal interaction, the surface of the mesoporous silica nanoparticles was functionalized through the reaction with (3-aminopropyl)-triethoxysilane (3-APTES) to produce functionalized aminopropyl-silica (NH_2-SiO_2). The 3-APTES was chosen with regard to the results of Chen et al. [12], displaying that among the various surface functionalizing groups, aminopropyls delivered the highest activity for BnOH oxidation of Pd° or Au-Pd alloy supported on mesoporous silica TUD-1. The role of the aminopropyl group is to act as a pseudo-chelator or binder to promote the interaction of the surface with metal precursors, or with metal NPs, in order to prevent metal leaching, and aggregation of metal particles during the reduction process [12]. According to the literature and depending on the surface area, a SiO_2/APTES = 1.55 molar ratio was adopted [24,25]. To confirm the success of the functionalization, the presence of the aminopropyl groups on the surface was verified by Fourier-transform infrared (FTIR) and X-ray photoelectron spectroscopy (XPS).

Pd° nanoparticles were prepared using oleylamine (Oam) as reducing agent (see Equation (1)), varying the reaction time and the ratio between Oam and the capping agent trioctylphosphine (TOP) [32], leading to formation of palladium NPs with different sizes (Figure S2, Supplementary Materials).

$$2PdCl_2 + C_{18}H_{35}NH_2 \rightarrow 2Pd^\circ + C_{17}H_{33}CN + 4HCl \quad (1)$$

The Pd° NPs with the lowest size were deposited on the functionalized support, leading to the production of a uniform powder, being dark in color when wet (Figure S3a, Supplementary Materials), and light grey when dried. This sample was named Pd°/NH_2-SiO_2. The deposition of Pd° NPs on NH_2-SiO_2 was proved by scanning electron microscopy (SEM), detailed in Section 2.2.2.

The Pd°/NH_2-SiO_2 was compared with a sample supporting Pd-P alloy, prepared using K_2PdCl_4 as Pd source, citric acid as complexing agent [33], and, $NaH_2PO_2 \cdot H_2O$ as reducing agent (Equation (2)) as well as phosphorous source (Equation (3)). $NaH_2PO_2 \cdot H_2O$, activates the in situ reduction of $PdCl_4^{2-}$ to Pd° and, the formation of the Pd-P alloy (Equation (4)) [34].

$$PdCl_4^{2-} + H_2PO_2^- + 3OH^- \rightarrow Pd^\circ + HPO_3^{2-} + 2H_2O + 4Cl^- \quad (2)$$

$$3H_2PO_2^- \rightarrow H_2PO_3^- + 2P + H_2O + 2OH^- \quad (3)$$

$$nPd^\circ + P \rightarrow Pd_nP \quad (4)$$

Pd-P alloy was successfully loaded on the NH_2-SiO_2 as support as later proved by SEM, transmission electron microscopy (TEM), and XPS (Sections 2.2.2 and 2.2.6, respectively). The final product (Figure S3b, Supplementary Materials) was named Pd-P/NH_2-SiO_2.

2.2. Catalyst Characterization

Morphological, structural and chemical composition of samples were studied by Brunauer–Emmett–Teller (BET) surface area analysis, Barrett–Joyner–Halenda (BJH) pore analysis, SEM, TEM, X-ray diffraction (XRD), FTIR, thermogravimetric and differential thermal analysis (TG-DTA), and XPS.

2.2.1. BET and BJH Morphological Analyses

BET surface area, BJH pore volume and BJH average pore size were measured for untreated SiO_2, functionalized silica (NH_2-SiO_2), and functionalized silica after deposition of metallic palladium (Pd°/NH_2-SiO_2) or a palladium-phosphorous alloy (Pd-P/NH_2-SiO_2). The corresponding values are listed in Table 1. Nitrogen adsorption–desorption isotherms of SiO_2 (Figure 1A), showed the type IV pattern with H1 hysteresis, characteristic of mesoporous materials with high surface area and narrow distribution of the meso-pore diameter [35,36]. The surface area of SiO_2 was 564 m^2 g^{-1}. The functionalization with aminopropyl groups considerably decreased the amount of N_2 physisorbed on the surface, whereas it did not affect the isotherm profile; the corresponding surface area was 88 m^2 g^{-1}. The subsequent addition of Pd° slightly changed the amount of N_2 physisorbed on the surface and did not affect the isotherm profile: the surface area was 110 m^2 g^{-1}. After adding the Pd-P on the NH_2-SiO_2, the amount of N_2 physisorbed on the surface increased and the surface area reached 235 m^2 g^{-1}. These findings may be explained by the Pd and Pd-P loading procedures causing a different decrease of the aminopropyl groups on the surface of catalysts. To verify this hypothesis, experiments of functionalization were performed varying 3-APTES concentration, maintaining unvaried temperature (110 °C) and time of reflux (48 h), finding that surface area decreased with 3-APTES concentration, due to different amount of aminopropyl groups on the surface (Table S1 in Supplementary Materials). Therefore, the different BET surface areas of Pd containing samples, are related to the different amount of aminopropyl groups on the surface due to their partial detachment from the surface during the dispersion of NH_2-SiO_2 in different volumes of solvent: 20 mL of cyclohexane, in Pd° loading procedure, or 88 mL of ethanol and water in Pd-P loading procedure.

Table 1. Morphological properties of the samples by Brunauer–Emmett–Teller (BET) surface area (S.A.) analysis, Barrett–Joyner–Halenda (BJH) pore analysis and scanning electron microscopy (SEM).

Technique Sample	BET S.A. (m^2 g^{-1})	BJH Pore Volume (cm^3 g^{-1})	BJH Pore Size (nm)	SEM Average Pd Particle Size (nm)
SiO_2	564	0.63	4.3	-
NH_2-SiO_2	88	0.17	10.8	-
Pd°/NH_2-SiO_2	110	0.06	3.6	12
Pd-P/NH_2-SiO_2	235	0.41	5.0	8

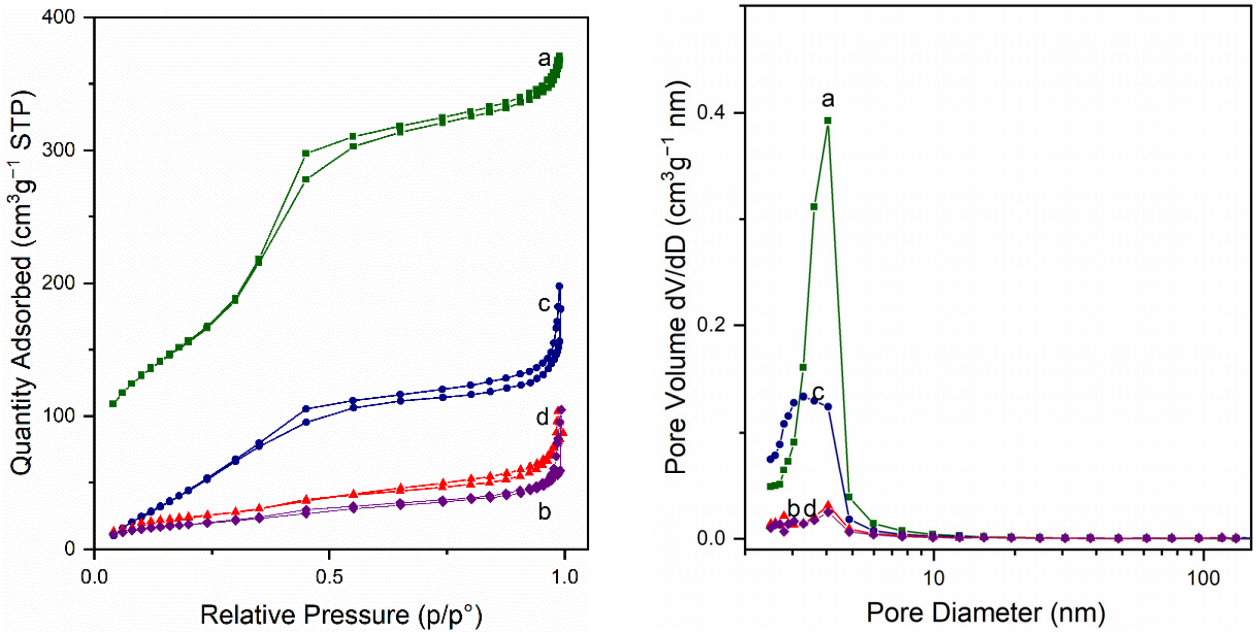

Figure 1. (**A**) N_2 adsorption and desorption isotherms, and (**B**) pore size distributions (PSD) of: (a) SiO_2, (b) NH_2SiO_2, (c) Pd-P /NH_2-SiO_2, (d) Pd°/NH_2-SiO_2.

The BJH pore size distribution of mesoporous SiO_2 support (Figure 1B) showed a narrow peak in the range of nanopores, at 3–5 nm, corresponding to a total pore volume of 0.63 cm^3 g^{-1}. The presence of aminopropyl groups on the surface, strongly decreased the total pore volume of silica by about 70%, maintaining a pore size distribution centered at 4.5 nm. The addition of Pd° caused an additional decrease of total pore volume up to about 10% of the initial pore volume in the pure SiO_2 support, in part due to partial occlusion of silica pores by Pd° loading on the surface. On the contrary, the deposition of Pd-P alloy caused an increase in the total pore volume of the catalyst up to 0.41 cm^3 g^{-1} and, a slight broadening of the profile of the pore size distribution below 3 nm.

2.2.2. SEM and TEM Morphological Characterization

The SEM images of the pure support SiO_2, and of the Pd°/NH_2-SiO_2 and Pd-P/NH_2-SiO_2 catalysts are displayed in Figure 2a–c, respectively. In all samples, silica particles are nearly spherical and homogeneous, with a narrow size distribution around 300 nm. The surface of the silica particles was not smooth, but rather wrinkled. The functionalization with aminopropyl groups and the subsequent addition of Pd° or Pd-P alloy did not significantly affect the shape and the morphology of SiO_2. Palladium and Pd-P alloy are visible as light small spherical particles. The Pd° and Pd-P average particle sizes are obtained as surface-weighted average diameter from almost 50 particles, using Equation (5), and

the values are reported in Table 1. The Pd average particle size in the Pd°/NH_2-SiO_2 was larger than those reported by Yang and Klabunde, for similar preparation method [32].

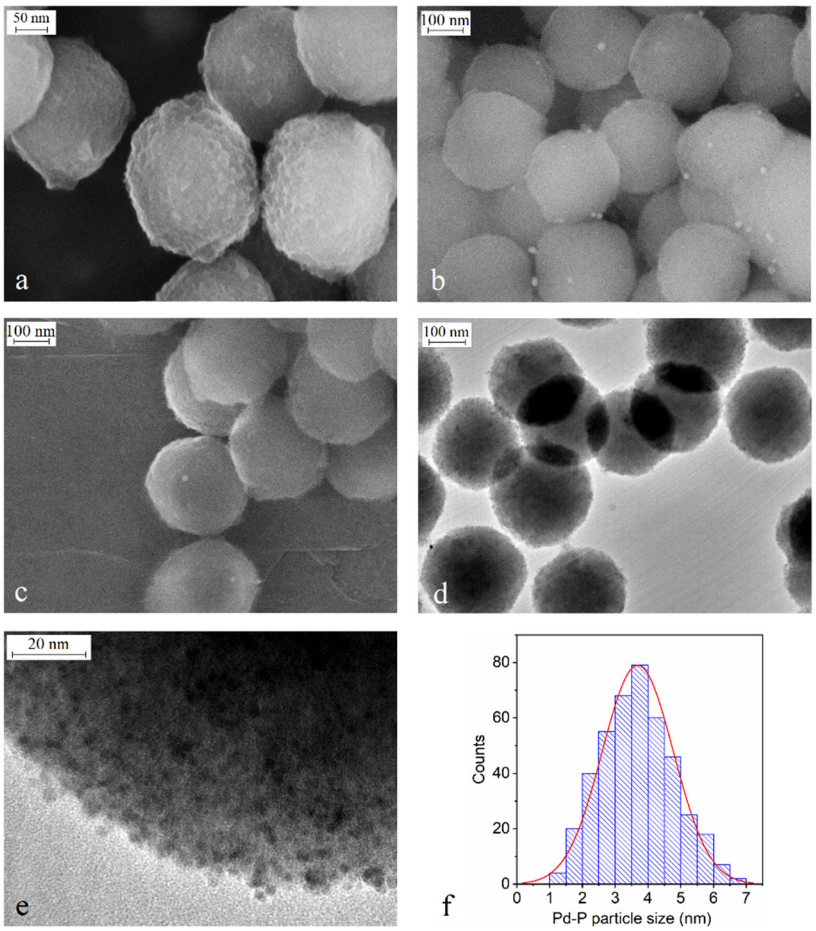

Figure 2. Electron microscopy of SiO_2, Pd°/NH_2-SiO_2 and Pd-P/NH_2-SiO_2: (**a**) SEM image of SiO_2, (**b**) SEM image of Pd°/NH_2-SiO_2, (**c**) SEM image of Pd-P/NH_2-SiO_2, (**d**) Transmission electron microscopy (TEM) image of Pd-P/NH_2-SiO_2, (**e**) enlarged TEM image of Pd-P/NH_2-SiO_2, (**f**) Pd-P particle size distribution calculated for 400 particles.

Further imaging of Pd-P/NH_2-SiO_2 was carried out by TEM to explore the presence of isolated aggregates of phosphorous species in addition to Pd-P alloy, and to confirm the particle size and the homogeneous distribution of palladium (Figure 2d,e).

The TEM images of Pd-P/NH_2-SiO_2 catalyst, with two different enlargements, are reported in Figure 2d,e. In good agreement with SEM images, silica particles have a diameter close to 300 nm. The Pd-P nanoparticles, recognizable as the small dark spots, are well dispersed on the silica surface. There is no evidence of isolated phosphorous aggregates. The histogram in Figure 2f shows the distribution of the particle size, related to approximately 400 particles, obtained by measuring the diameter with the software ImageJ. Most of the particles have a diameter in the range 2.5–5.0 nm, with an average size of 3.7 nm, corresponding to a dispersion D (%) = 32. The difference between the average particle size evaluated from SEM or TEM analysis of Pd-P/NH_2-SiO_2 sample, is probably due to the higher resolution of the TEM images, reducing the uncertainty in the measurement of the diameter of smaller nanoparticles.

2.2.3. XRD Structural Characterization

XRD patterns of pure SiO_2, NH_2-SiO_2, Pd°/NH_2-SiO_2 and Pd-P/NH_2-SiO_2 are reported in Figure 3. All patterns show a broad peak, with the maximum at 2θ = 22°, characteristic of amorphous silica (JCPDS n°. 29–0085). Neither Pd°/NH_2-SiO_2 nor Pd-P/NH_2-SiO_2 samples

show Pd° diffraction lines (Figure 3), whose most intense one, corresponding to the (111) plane, should be at 41° (JCPDS n°. 05–0681). Conversely, palladium is clearly revealed by TEM and XPS analysis. These results indicate that palladium crystallite size is below the XRD detection limit due to the low crystallinity and to the low concentration of the phase.

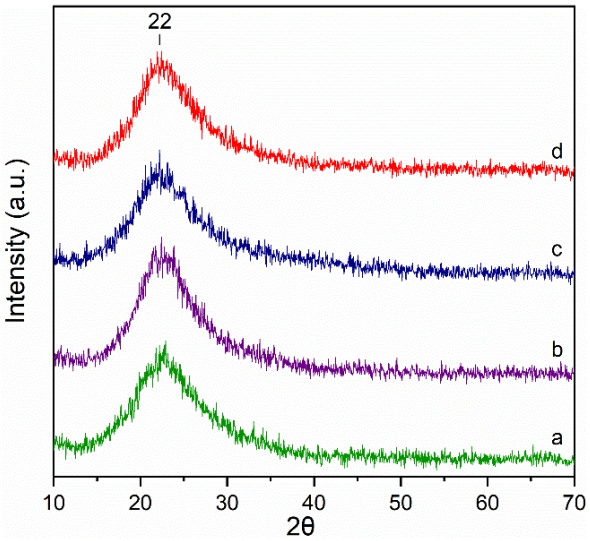

Figure 3. X-ray diffraction (XRD) patterns of samples: (a) SiO_2, (b) NH_2-SiO_2, (c) Pd-P/NH_2-SiO_2, (d) Pd°/NH_2-SiO_2.

2.2.4. FTIR Spectroscopy

The effectiveness of silica functionalization was investigated by FTIR spectroscopy. Figure 4 shows FTIR spectra of the support, pure and functionalized, and of the Pd containing catalysts. The spectrum of pure silica support (spectrum a) showed: a broad peak at 3445 cm^{-1} and a peak at 1638 cm^{-1} assigned to the O-H stretching of silanol groups and to the bending of physically adsorbed water, respectively; a strong peak at about 1100 cm^{-1}, peaks at 800 cm^{-1} and 468 cm^{-1}, assigned to the asymmetric and symmetric stretching, and to bending vibrations of the framework (Si-O-Si), respectively; a peak at 965 cm^{-1} attributed to the asymmetric stretching of silanol bond Si-OH.

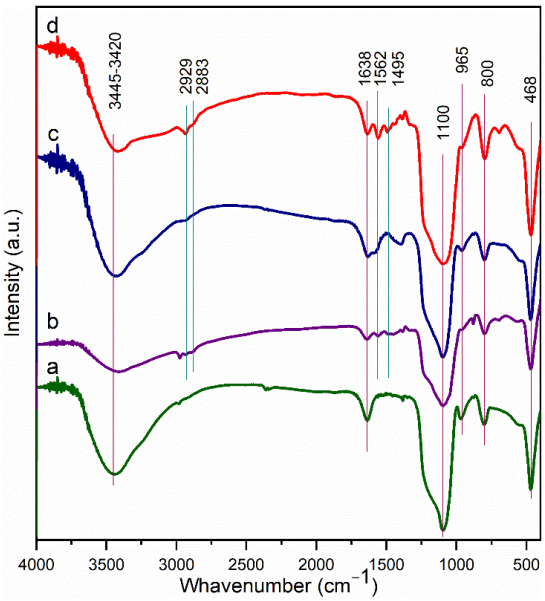

Figure 4. FTIR spectra of: (a) SiO_2, (b) NH_2-SiO_2, (c) Pd-P/NH_2-SiO_2, (d) Pd°/NH_2-SiO_2.

The spectrum of aminopropyl-modified silica (spectrum b) additionally shows peaks at 2929 and 2883 cm^{-1}, assigned to the stretching vibrations of the $–CH_2$ group, a peak at 1562 cm^{-1} assigned to the bending vibration of N-H bond, and a peak at 1495 cm^{-1} assigned to the bending of $–CH_2$ groups, proving that functionalization has occurred. In addition, we can observe a decrease in the relative intensity of the band of the surface silanols at 965 cm^{-1}, suggesting a successful anchoring of 3-APTES, as observed by other authors [37]. The observed FTIR bands are summarized in Table 2. The bands due to the aminopropyl groups are not very intense, given the low concentration of these surface species. The difference in the intensity of spectra may be due to inhomogeneous concentration of the samples in the KBr tablet.

Table 2. FTIR bands of samples.

Wave Number (cm^{-1})	Vibration
3445–3420	Stretching O-H
2929, 2883	Stretching CH_2
1638	Bending H_2O
1562	Bending NH_2
1495	Bending CH_2
1100–1045	Asymmetric stretching Si-O-Si
965	Stretching Si-OH
800	Symmetric stretching Si-O-Si
468	Bending Si-O-Si

After the loading of Pd° or Pd-P, the bands assigned to the adsorbed aminopropyl groups are still present (spectra c and d), indicating that the Pd addition does not eliminate the aminopropyl groups on the surface.

2.2.5. TG-DTA Analysis

TG-DTA analysis was performed to study the thermal stability of the aminopropyl groups on the surface. Thermogravimetric analysis (TG) of functionalized support NH_2-SiO_2 (Figure 5A, curve a) shows a rapid weight loss of about 8% below 125 °C, corresponding to a negative peak (endothermic) in the differential thermal analysis (DTA) (Figure 5B, curve a), which is due to dehydration. Afterwards, the sample remains stable until 300 °C and then shows a further weight loss of about 20% of the initial mass, heating up to 700 °C. This further weight loss is attributed to the oxidative decomposition and desorption of the aminopropyl groups from the surface. In agreement with this, the corresponding DTA profile shows an exothermic process corresponding to oxidation reaction in the range 250–470 °C with a strong peak at 300 °C.

TG profiles of Pd°/NH_2-SiO_2 and Pd-P/NH_2-SiO_2 catalysts show a similar progressive weight loss of about 20% of the initial weight, heating from 30 up to 600–700 °C. For both samples, the total weight loss is attributed to the oxidative decomposition and desorption of aminopropyl groups and of palladium and phosphorus compounds. The corresponding DTA curves (Figure 5B) of Pd°/NH_2-SiO_2 and Pd-P/NH_2-SiO_2 samples show a more complex profile of exothermic processes in comparison with the bare functionalized support. In particular, (i) both samples show a peak at about 200 °C, tentatively attributed to Pd oxidation; (ii) Pd-P/NH_2-SiO_2 does not show the intense peak at 300 °C, suggesting the presence of a lower amount of aminopropyls on the surface, consistent with BET analysis; (iii) Pd-P/NH_2-SiO_2 shows a peak at about 520 °C, which is absent or very weak in the Pd°/NH_2-SiO_2 sample; therefore, it is attributable largely to phosphorous species.

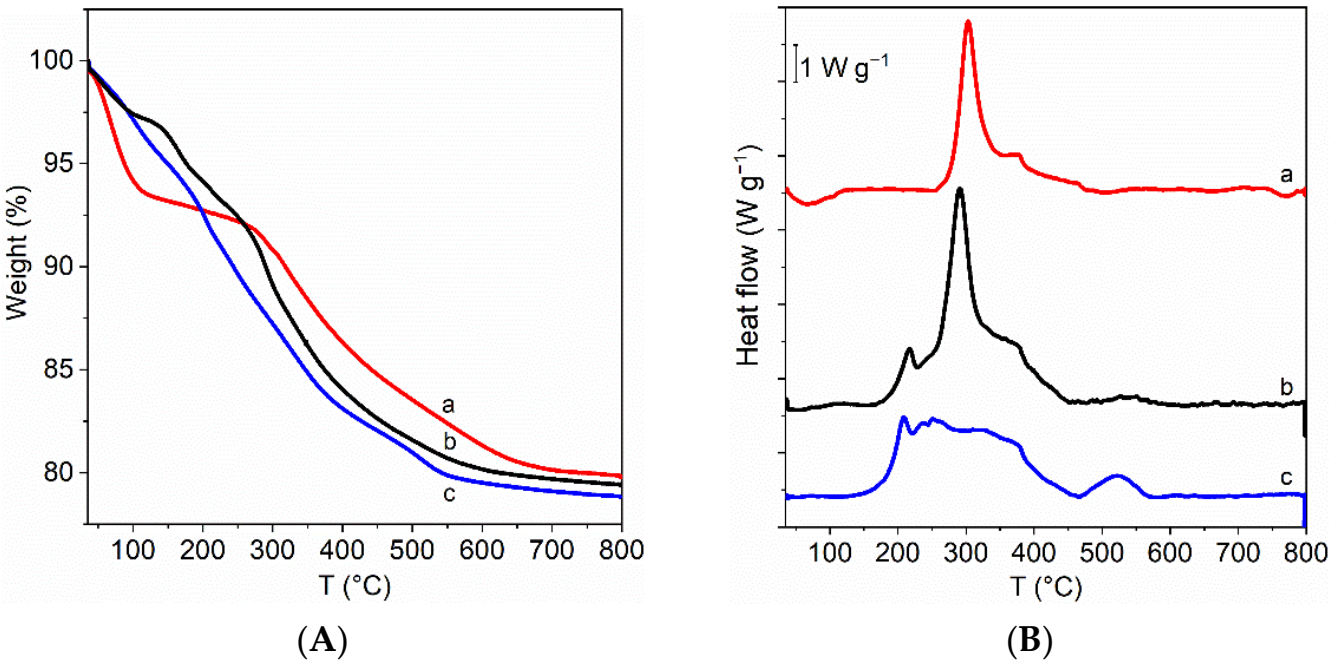

Figure 5. (**A**) Thermogravimetric (TG) analysis, as sample weight (%) versus temperature, (**B**) differential thermal analysis (DTA) as heat flow (W g^{-1}) versus temperature patterns of samples: (a) NH_2-SiO_2, (b) Pd°/NH_2-SiO_2, (c) Pd-P/NH_2-SiO_2.

2.2.6. XPS Characterization

The XPS analysis was carried out to investigate the atomic composition of the surface, focusing on nitrogen element, derived from aminopropyl groups, for both NH_2-SiO_2 and Pd-P/NH_2-SiO_2 samples, and on palladium and phosphorous elements for the Pd-P/NH_2-SiO_2 sample. The binding energies (BE) of O 1s, C 1s, N 1s, Si 2p, P 2p and Pd 3d (both spinning 5/2 and 3/2) are compiled in Table 3.

Table 3. Binding energies (eV) of the core levels in XPS spectra.

Samples	O 1s	C 1s	Pd 3d (5/2)	Pd 3d (3/2)	P 2p	N 1s	Si 2p
NH_2-SiO_2	532.96 (528.88)	285.22	-	-	-	399.92	103.49
Pd-P/NH_2-SiO_2	532.99 (530.15)	285.00	335.28 337.55 [1]	340.37 342.22 [1]	130.39	399.77	103.57

[1] Relative to the palladium(II) species.

The broad XPS spectra of the Pd-P/NH_2-SiO_2 catalyst and the functionalized support, Figure 6a, display intense peaks for Si 2s, Si 2p, N 1s, C 1s, and O 1s, proving the presence of silica and aminopropyl groups, and the success of the 3-APTES functionalization [38]. For Pd-P/NH_2-SiO_2 sample, presence of palladium and phosphorous is confirmed by the identified Pd 3d and P 2p signals, even though only weak peaks were detected.

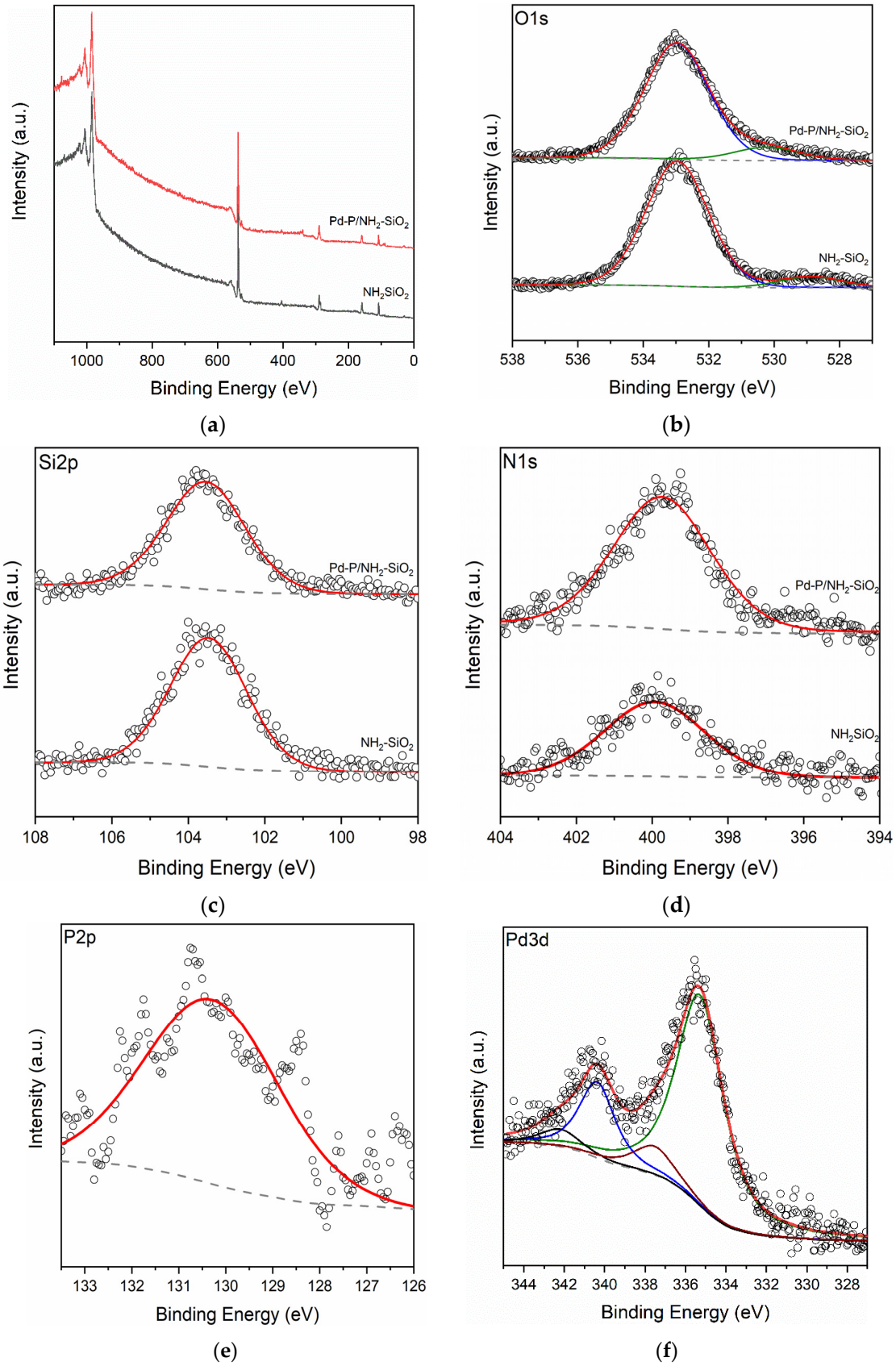

Figure 6. X-ray Photoelectron Spectroscopy (XPS) spectra for NH_2-SiO_2 and Pd-P/NH_2-SiO_2: (**a**) complete range, and regions of (**b**) O 1s, (**c**) Si 2p, (**d**) N 1s, (**e**) P 2p, (**f**) Pd 3d core levels.

The NH_2-SiO_2 and Pd-P/NH_2-SiO_2 samples show the oxygen main peak O 1s, assigned to the oxygen bond of Si-O-Si in the bulk of silica, at 532.96 eV and 532.99 eV, respectively (Figure 6b). The secondary peaks of O 1s, at 528.88 eV and 530.15 eV, are due to oxygen bonded to carbon, or phosphorous and/or palladium. For both samples, the Si 2p, related to the silicon of the SiO_2, was fitted by a single peak (Figure 6c) at 103.49 eV and 103.57 eV, respectively [38]. The C 1s peaks highlight the presence of residual organic compounds, probably due to the 3-APTES on both samples. For this reason, O 1s was taken as a reference for the correction of the binding energies instead of C 1s, which is generally used as reference in XPS analysis.

The N 1s spectra (Figure 6d), showing a single peak at around 400 eV, underline that the main component of the nitrogen signal is due to the aminopropyl groups, confirming that the silica support is functionalized. The slight binding energy difference between the two samples (Δ(BE) = 0.15 eV) could be attributed to an electronic variation due to the interaction of the Pd-P alloy with the aminopropyl group.

The P 2p spectrum of Pd-P/NH_2-SiO_2 (Figure 6e) shows a prominent peak of phosphorus at 103.39 eV, attributed to the elemental red phosphorous P^0 [39]. The spectrum noise impeded the detection of any possible BE difference between the isolated elemental phosphorus and the bonded phosphorus in the alloy, as reported by Lu et al. [40], arising from transfer of electrons from Pd to P. However, Belykh et al. [41] reported a BE value for phosphorus interacting with metallic palladium in alloy, similar to that reported in the present research, in addition to a peak at higher binding energy, relative to oxidized phosphorous of phosphates derived by the reduction process of NaH_2PO_2, which are common in Pd-P alloy prepared by precipitation-reduction method [40,42,43]. Furthermore, the elemental states of phosphorous and palladium reveal that both elements underwent a reduction during the synthesis.

The Pd 3d spectrum (Figure 6f) shows two asymmetric peaks originated by the partial overlapping of peaks of Pd° at 335.28 and 340.37 eV with the less intense peaks of some electron-depleted palladium(II) at 337.55 and 342.22 eV, corresponding to Pd $3d_{5/2}$ and Pd $3d_{3/2}$, respectively. These values are in good agreement with the expected values for the Pd° and Pd(II) reported in literature [10,44]. The total amount of Pd(II) was estimated from the deconvoluted areas to be 13% of the total palladium content, suggesting that the catalyst was partially oxidize on the surface possibly due to the exposure to air before XPS analysis.

The elemental composition on the surface of the catalysts, determined by XPS analysis as atomic percentage, is reported in Table 4. Carbon was not considered when calculating the atomic percentage of the elements, since its presence could be related both to the surface aminopropyl groups, and/or to contaminants adsorbed on the catalyst surface.

Table 4. XPS atomic percentage of the elements.

Sample	O 1s (%)	Pd 3d (%)	P 2p (%)	N 1s (%)	Si 2p (%)
NH_2-SiO_2	62.0	-	-	5.7	32.3
Pd-P/NH_2-SiO_2	70.9	1.2	0.6	3.2	24.1

The atomic ratio Pd/P = 1.2/0.6 = 2 suggests the formation of a Pd-P alloy with a stoichiometric excess of Pd. Among various stable Pd-P alloys [45], Pd_5P_2 and Pd_3P have a composition close to the measured atomic ratio. The formation of these species was observed by other authors on samples prepared with a procedure similar to that used in this work [39,46].

2.3. Catalytic Tests

The catalytic activity of the synthesized catalysts for the BnOH oxidation was studied. The reaction was performed in different solvents (ethanol, acetonitrile, and toluene), using various temperatures, and two different BnOH concentrations. Air was generally used

as oxidant but a test with pure O_2 was also performed to check the effect of the oxygen concentration. Table 5 outlines the reaction parameters and results of Pd°/NH_2-SiO_2 and Pd-P/NH_2-SiO_2 preliminary catalytic tests.

Table 5. Oxidation of benzyl alcohol (BnOH) to benzaldehyde (PhCHO); effect of solvent.

Entry	Catalyst	Solvent	T (°C)	BnOH Conversion (%) [1]	PhCHO Selectivity (%) [1,2]
1	Pd°/NH_2-SiO_2	Ethanol	78	<5	N/A
2	Pd°/NH_2-SiO_2	Toluene	111	<5	N/A
3	Pd-P/NH_2-SiO_2	Ethanol	78	7	96
4	Pd-P/NH_2-SiO_2	Acetonitrile	82	29	96
5	Pd-P/NH_2-SiO_2	Toluene	80	38	94

[1] Measured by GC-MS after 5 h of BnOH oxidation: 10 mL of BnOH solution (16 mM); 32 mg catalyst with BnOH (mole)/catalyst (g) ratio of 1:200; 20 mL min^{-1} air flow. [2] Calculated solely for reactions with ≥5% conversion.

Pd°/NH_2-SiO_2 was rather inactive both in ethanol and in toluene at the respective boiling points of the solvents (Table 5, Entry 1 and 2, respectively), whereas Pd-P/NH_2-SiO_2 sample was active in toluene and acetonitrile (Table 5, Entry 4 and 5, respectively) and poorly active in ethanol (Table 5, Entry 3). Therefore, the presence of phosphorous could play an essential role in the catalytic activity of the synthesized samples. One reason for the Pd°/NH_2-SiO_2 inactivity might be the relatively large particle size of palladium, i.e., 12 nm (Table 1). This hypothesis might be strengthened by considering the observation of Chen et al. [47], who showed that enlargement of the Pd particle size in a Pd/SiO_2-Al_2O_3 catalyst from almost 4 up to 10 nm caused an approximately 85% decrease in TOF for BnOH oxidation.

Regarding the activity of Pd-P/NH_2-SiO_2 sample, in addition to the smaller particle size compared with Pd°/NH_2-SiO_2, role of phosphorous in the catalytic activity must be taken into account. In the Pd-catalyzed BnOH oxidation mechanism suggested by Savara et al. [15,18,48,49], the metallic palladium causes the hydrogen abstraction from the generated alkoxide–palladium bond, leading to the release of PhCHO. Guo et al. displayed that the BnOH conversion by Pd-P alloy supported on PCF was approximately three times of the conversion acquired by single palladium deposited on the same support [10]. It seems that the presence of phosphorous may reduce the 3d electron density of palladium, facilitating the desorption of the product and therefore maintaining the catalytic activity [10,20,50]. This could also explain the significant increase of catalytic activity obtained in the present study. XPS analysis proved the presence of elemental phosphorous with atomic ratio Pd/P = 1.2/0.6 on the surface; in addition, no evidence of aggregated phosphorous particles was observed in TEM images of Pd-P/NH_2-SiO_2. These, along with the possible electronic interaction among Pd and P insinuated by the catalytic activity, could further strengthen the suggestion that phosphorous and palladium formed an alloy on the surface of the functionalized silica.

Furthermore, the catalytic performance of Pd-P/NH_2-SiO_2 was significantly influenced by the nature of the solvent, reaching 7, 29, and 38% BnOH conversion in ethanol, acetonitrile, and toluene, respectively. The very low catalytic activity in ethanol (Table 5, Entry 3) might be attributable to a competition between the alcoholic substrate and the alcoholic solvent for interacting with the catalyst [51]. On the other hand, the adsorption of BnOH on the surface of the catalyst could be facilitated by the less solvating non-protic toluene, because, in these conditions, the H-bonding could only be formed between BnOH and -NH_2 groups on the silica surface. The reason of the different catalytic activity in acetonitrile and toluene (Table 5, Entry 4 and 5) might be the higher oxygen solubility in toluene [52,53]. Furthermore, in comparison with the non-polar toluene, the polar nature of acetonitrile may pose an adverse effect on the catalytic oxidation of BnOH. The reason is that BnOH is polar itself, which itself and could interacts more strongly with acetonitrile than with toluene. This might lead to slower catalyst/substrate interaction in acetonitrile than in toluene.

Toluene was chosen to check the effect of temperature and oxygen concentration on the catalytic activity and selectivity of Pd-P/NH_2-SiO_2 because the best activity was obtained in this solvent and, it could provide the opportunity of performing the reaction at higher temperatures, The reaction conditions and outcomes are reported in Table 6, and Figure 7. BnOH conversion after 5 h raised from 11% at 50 °C to 24% at 80 °C, and remarkably up to 57% at 111 °C. This is in line with the general trend of catalytic BnOH oxidation [18], and has been observed in other studies [9,54].

Table 6. Oxidation of BnOH in toluene over Pd-P/NH_2-SiO_2 catalyst; effect of temperature and oxidant nature.

Entry	T (°C)	Oxidant (20 mL min^{-1})	BnOH Conversion (%) [1]	PhCHO Selectivity (%) [1]	TOF (h^{-1})
1	50	Air	11	65	55
2	80	Air	24	95	255
3	111	Air	57	63	4999
4	111	O_2	78	66	5982

[1] Measured by GC-MS after 5 h of BnOH oxidation: 10 mL of BnOH solution (0.1 M); 53 mg Pd-P/NH_2-SiO_2 catalyst with BnOH (mole)/Catalyst (g) ratio of 1:53.

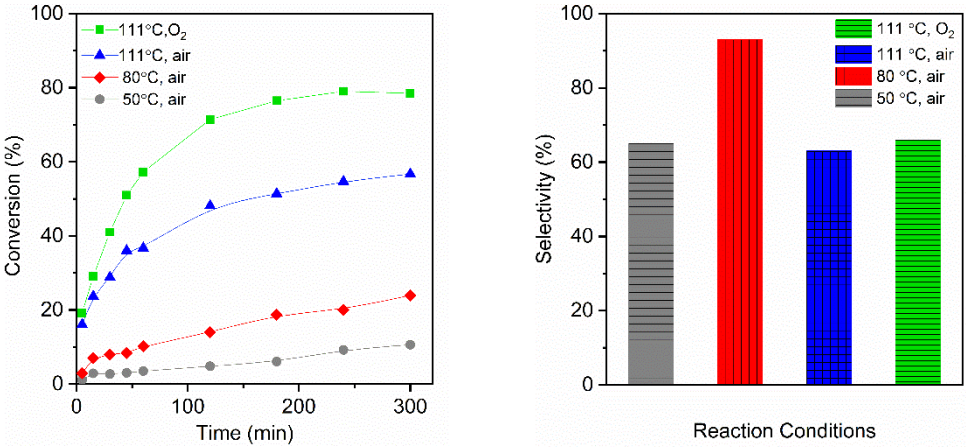

(**a**) (**b**)

Figure 7. Catalytic activity of Pd-P/NH_2-SiO_2: (**a**) effect of temperature and oxidant on BnOH conversion over time, (**b**) PhCHO selectivity at 5 h. Reaction conditions: 10 mL BnOH (0.10 M) solution in toluene, 53 mg Pd-P/NH_2-SiO_2 and 20 mL min^{-1} oxidant flow rate.

On the other hand, when using air as oxidizing agent, selectivity towards PhCHO showed a bell-shaped behaviour: climbing from 65 to 95% by increasing the temperature from 50 to 80 °C and falling back to 63% by a further rise in temperature to 111 °C (Figure 7b). The absence of peaks of any by-product in the gas-chromatograms suggests that the secondary products could be those impossible to be detected by GC-MS, i.e., toluene or benzene. The decline in PhCHO selectivity at higher temperatures can be explained by boosted toluene production, as the activation barrier of formation of toluene through C—O bond cleavage is higher than that of benzaldehyde [55]. It is noteworthy that despite the decrease in selectivity from 80 to 111 °C, the yield of PhCHO increased from 23 to 36%, due to the sharp rise in the conversion.

BnOH conversion considerably increased from 57 to 78% through replacement of air by O_2 (Table 6, Entry 3 and 4). This occurred along with preservation and even a slight enhancement of PhCHO selectivity, and without any over-oxidation of PhCHO to benzoic acid, resulting in 52% PhCHO yield. This is congruent with the general trend of Pd-catalyzed BnOH oxidation which assumes an increase in conversion and selectivity following the rise in oxygen pressure [18], because the consequent enhancement of oxygen solubility promotes the release of PhCHO and suppresses the toluene formation [15]. In

short, elevating the reaction temperature and increasing the partial pressure of oxygen uplifted the yield of PhCHO production.

The recyclability of Pd-P/NH_2-SiO_2 was examined at 111 °C using 20 mL min^{-1} air. The results (Figure S4) showed that the catalyst remained active for the second and the third rounds of the reaction, just by a simple separation and washing. Although the value of the yield decreased from the first to the third round (from 36 to 28%), the catalyst still preserved most of its activity.

The TOFs of Pd-P/NH_2-SiO_2 were calculated via Equation (10) and are reported in Table 6 (details provided in Section 3.3 and Table S2). Predictably, the highest TOF was observed in the experiment with the largest conversion (Table 6 Entry 4, TOF = 5982 h^{-1}, T = 111 °C, 20 mL min^{-1} O_2). Increasing the temperature from 50 up to 111 °C led to a significant raise of TOF from 55 to 4999 h^{-1}. In addition, a quasi-TOF (TOF_{bulk}) was calculated for each experiment using Equation (11), which omitted the effect of metal dispersion (Section 3.3 and Table S2). The values were expectedly smaller and followed the same trend as that of TOF values.

Comparing the catalytic results of this research with others was rather challenging because, despite the large volume of literature on BnOH catalytic oxidation, no research work was found with completely similar reaction conditions. The comparison was focused on articles that used the same metal on similar functionalized supports. The values of TOF were chosen to correlate the catalytic activities. The TOFs of four supported palladium catalysts are reported in Table 7 along with those of Pd-P/NH_2-SiO_2 and Pd°/NH_2-SiO_2. The Pd/PCF catalytic system (ref. [10] in Table 7) was chosen because of being the only support utilized for BnOH oxidation catalyzed by Pd-P. The TOF of Pd-P/NH_2-SiO_2 seemed to be comparable to that of the Pd-P alloy supported on PCF [10], which itself was higher than the TOF of metallic Pd supported on the same carbon frame, highlighting the favorable influence of alloying Pd with phosphorous [10]. In addition, the TOF of Pd-P/NH_2-SiO_2 looks comparable to that of Pd supported on aminopropyl-functionalized TUD-1 [12] or SBA-16 [29] silica catalysts. The considerably higher activity of the silica-supported palladium catalysts in Table 7 compared with Pd°/NH_2-SiO_2 of this study might be due to the significantly smaller Pd particle size in 1Pd/1.2APS-TUD (1.9 ± 0.2 nm) and Pd/APS-S16 (2.8 nm) in comparison with the 12 nm Pd particle size in Pd°/NH_2-SiO_2.

Table 7. TOF Comparison for Pd-P/NH_2-SiO_2 and other catalysts in the literature.

Catalyst	Support	Reaction Conditions	O_2 (mL min^{-1})	T (°C)	TOF (h^{-1})	Reference
Pd-P/NH_2-SiO_2	aminopropyl-functionalized mesoporous SiO_2	Solution	20	111	5982	This study
Pd°/NH_2-SiO_2					<700	
1Pd/1.2APS-TUD	aminopropyl-functionalized TUD-1 silica	Solvent free	20	100	2316	[12]
				120	3251	
Pd/APS-S16	aminopropyl-functionalized SBA-16 silica	Solvent free	20	100	~5600	[29]
				110	~6070	
Pd/PCF	porous carbon frame	Solvent free (continuous flow)	5	70	2147	[10]
Pd-P/PCF					6289	

3. Materials and Methods

3.1. Catalyst Synthesis

3.1.1. Materials

Mesoporous silica (STREM Chemicals U.S., Newburyport, MA, USA); oleylamine (OAm, Sigma-Aldrich U.S., St. Louis, MO, USA); trioctylphosphine (TOP, Sigma-Aldrich U.S.), palladium(II) chloride ($PdCl_2$, Sigma-Aldrich U.S.); (3-aminopropyl)-triethoxysilane (3-APTES, Sigma-Aldrich U.S.); toluene (Sigma-Aldrich U.S.); ethanol (Sigma-Aldrich U.S.); acetonitrile (Sigma-Aldrich U.S.); diethyl ether (Sigma-Aldrich U.S.); Celite (Standard Super Cel® fine-filter aid, calcined; Sigma-Aldrich U.S.); citric acid (Sigma-Aldrich U.S.); sodium hydroxide (NaOH, Sigma-Aldrich U.S.); n-dodecane (Sigma-Aldrich U.S.); potassium tetra-

chloropalladate(II) (K_2PdCl_4, Sigma-Aldrich U.S.); sodium hypophosphite monohydrate ($NaH_2PO_2 \cdot H_2O$, Alfa Aesar U.S., Haverhill, MA, USA).

3.1.2. Functionalization of Silica by Aminopropyl Groups

Commercial mesoporous silica was functionalized by adding aminopropyl groups on the surface according to the following procedure: 1.00 g (16.6 mmol) of mesoporous silica, 100 mL of toluene and 2.50 mL of 3-APTES (10.7 mmol; molar ratio SiO_2/3-APTES = 1.55) were stirred under argon flow at reflux for 48 h; then, the mesoporous silica was washed and centrifuged with water and ethanol, and finally dried in air at room temperature (RT) overnight [25]. The obtained functionalized silica was named NH_2-SiO_2.

3.1.3. Synthesis of Pd° NPs

First, 35.5 mg (0.20 mmol) of $PdCl_2$, 20 mL (60.80 mmol) of OAm and 0.10 mL of TOP (0.22 mmol) were added in a flask and heated under stirring up to 200 °C in argon flow for 1 h. A gradual colour changing from light yellow to brown and finally to black, was observed during the treatment, indicating the nucleation and subsequent growth of Pd° particles. Then, the Pd° nanoparticles (NPs) were extracted from the solution by adding 50 mL of isopropanol, followed by centrifugation. The Pd° NPs were further washed and dispersed in 10 mL of cyclohexane [32].

3.1.4. Deposition of Pd° NPs on NH_2-SiO_2

In order to deposit 2.0 wt.% Pd° NPs over NH_2-SiO_2, 250 mg of NH_2-SiO_2 were dispersed in 20 mL of cyclohexane and subjected to ultrasonication for 1 h. Then, one-fourth of the Pd° NP dispersion (from Section 3.1.3) was diluted to 5 mL with cyclohexane and added to support dispersion, followed by 1 h of ultrasonication. The resulting solid was finally washed with ethanol, separated by centrifugation, and air-dried overnight at RT. The sample was designated as Pd°/NH_2-SiO_2.

3.1.5. Loading Pd-P Alloy on NH_2-SiO_2

Totals of 810 mg (4.2 mmol) of citric acid, 18 mL of ethanol, and 460 mg (11.5 mmol) of NaOH were added to 70 mL of water and mixed by stirring to obtain sodium citrate. Then, 31.3 mg of K_2PdCl_4 (0.1 mmol), corresponding to 2.0 wt.% of Pd in the final catalyst, was added to the solution under stirring. Next, 500 mg of functionalized silica (NH_2-SiO_2) was added, and the obtained mixture was maintained under stirring for 2 h. Finally, 510 mg of $NaH_2PO_2 \cdot H_2O$ (4.8 mmol) was dissolved in 50.0 mL of water, and dropped into the mixture under stirring, which was continued for 4 h at 80 °C, causing the in situ reduction to produce Pd° and the formation of the Pd-P alloy. The precipitate was washed with water and ethanol several times and dried overnight in air at RT. The sample was named Pd-P/NH_2-SiO_2.

3.2. Characterization Technics

The surface area (S.A.) of the material was measured by N_2 adsorption–desorption isotherms at −196 °C using a Micromeritics Gemini V apparatus. Before the measurement, 0.020 g of sample was degassed at 200 °C in He flow for 2 h. The surface area was calculated by BET method in the equilibrium pressure range of $0.05 < p/p° < 0.3$. The pore size distribution was calculated from the desorption branch of the isotherms by BJH method, and the total pore volume was calculated from the maximum adsorption point at $p/p° = 0.98$. Catalyst morphology was studied by a Zeiss Sigma 300 VP-FESEM set-up with an accelerating voltage of 20 kV and a working distance of 4.0 mm, equipped with a high-resolution secondary electron detector (in-lens detector), and with energy-dispersive detector (EDS) that can provide a reasonable quantification of elements heavier than carbon. The powder was dispersed in isopropyl alcohol and ultrasonicated for 15 min. Then, a drop of the suspension (~20 µL) was placed on a sample holder with thin graphite film.

TEM was employed to evaluate the dispersion and the particles size of palladium using a JEM 200CX (JEOL, Peabody, MA, USA) instrument operating at 200 kV. The powder was dispersed in isopropyl alcohol and ultra-sonicated for 15 min. Then, a drop of the suspension (~20 µL) was placed on a copper TEM grid (400 mesh), covered by an amorphous carbon film. The surface-weighted average diameter $\bar{d}(nm)$ of Pd° or Pd-P species was calculated from the number of particles N_{d_i} with a diameter d_i according to Equation (5), by measuring the diameter with the software ImageJ:

$$\bar{d}(nm) = \frac{\sum_n^{i=1} N_{d_i} \times d_i^3}{\sum_n^{i=1} N_{d_i} \times d_i^2} \quad (5)$$

The dispersion D(%) of Pd° or Pd-P species was calculated according to Equation (6):

$$D(\%) = 6 \times 10^9 \cdot \frac{V_{Pd}}{A_{Pd}} \cdot \frac{1}{\bar{d}} \quad (6)$$

where V_{Pd} is the volume of a Pd atom in bulk metal (1.47×10^{-23} cm^3) and A_{Pd} is the area of a Pd surface atom 7.93×10^{-16} cm^2 (see Table 2 in [56]).

FTIR analysis was performed by Thermo Nicolet nexus, Spectrum 100. Powder was diluted in KBr and pressed as tablet at 2 Tons.

XRD patterns were recorded using a Scintag X1 diffractometer equipped with a Cu Kα (λ = 1.5418 Å) source and the Bragg–Brentano θ–θ configuration in the 2θ = 10–80 range, with 2θ = 0.05° step size and 1 s acquisition time.

TG-DTA analyses were performed by a Mettler Toledo TGA/DSC1 Star System, heating 7 ± 0.5 mg of sample from 30 up to 800 °C with a ramp of 10 °C min^{-1} in a mixture of 70 cm^3 min^{-1} of synthetic air and 30 cm^3 min^{-1} of N_2.

The elemental surface composition of the samples was determined by XPS. The powder was pressed into pellets, and the measurement was carried out with a VG Escalab MkII Spectrometer using Alka X-ray emission (1486.6 eV). A reference gold wire was placed on the pellet to account for possible sample charging. The XPS chamber is equipped with oil-free pumps to avoid carbon contaminations, and the measurement was performed in a base vacuum of 3.0×10^{-9} mbar. Photoelectrons emitted by C 1s, N 1s, O 1s, Si 2p, and Pd 3d and P 2p core levels were detected; the corresponding peaks in the spectra were fitted with a Shirley background and Lorentzian–Gaussian peak functions. Energy resolution of binding energies are reported after correction for charging, using O 1s as a reference at BE 533.0 eV oxygen in the Si-O-Si bond [57].

3.3. Catalytic Test

The activity of the catalysts for the BnOH oxidation reaction was investigated using a 25 mL three-neck flask, fitted with reflux condenser and thermometer. A pre-heated silicon oil bath was utilized to heat the flask and reactants. Air or pure oxygen was bubbled onto the reaction mixture at rate of 20 cm^3 min^{-1} through a mass flow controller, while maintaining continuous and vigorous stirring. The reaction was performed using either 10 mL of 0.016 M BnOH solution and 32 mg of catalyst, or 10 mL of 0.1 M BnOH solution and 53 mg of catalyst, varying solvent nature, temperature, and oxidizing agent (Tables 5 and 6). The reaction was monitored via a Shimadzu VG 70/250S GC-MS, equipped with a Supelco SLB™ column (30 m, 0.25 mm, and 0.25 m film thickness). The GC-MS analysis started at 50 °C, then raised up to 250 °C (10 °C min^{-1} temperature gradient). To remove the catalyst and adjust a proper concentration for GC-MS analysis, each sample taken from the reactions was passed through a celite filter being eluted with diethyl ether. N-dodecane was utilized as the internal standard to monitor the changes in the concentration of BnOH

and the products during the reaction. BnOH conversion and PhCHO selectivity are defined in Equations (7) and (8), respectively.

$$\text{Conversion } (\%) = \frac{\text{moles of benzyl alcohol reacted}}{\text{initial moles of benzyl alcohol}} \times 100 \quad (7)$$

$$\text{Selectivity } (\%) = \frac{\text{moles of benzaldehyde produced}}{\text{moles of benzyl alcohol reacted}} \times 100 \quad (8)$$

The yield of PhCHO was calculated from the conversion and selectivity via Equation (9)

$$\text{Yield } (\%) = \frac{\text{Conversion} \times \text{Selectivity}}{100} \quad (9)$$

TOF was calculated from BnOH conversion below 20%, by the following Equation (10)

$$\text{TOF } \left(\text{h}^{-1}\right) = \frac{\text{n} \cdot \text{X}}{\text{D} \cdot \frac{\text{m}_{\text{Pd}}}{\text{M}_{\text{Pd}}} \cdot \text{t}} \quad (10)$$

where n is the initial moles of benzyl alcohol, X (%) is the benzyl alcohol conversion, D (%) is the Pd dispersion by TEM analysis and Equation (6) (32%), m (g) is the mass and M (g) is the molar mass of Pd (g mol^{-1}), *t* is the reaction time (h). Pd content was estimated by SEM-EDS (0.91 $\pm$ 0.23%w/w). More details about the calculations of TOF are reported in Table S2.

In addition, turnover frequency of Pd-P/NH_2-SiO_2 based on total Pd content (TOF_{bulk}) was calculated by Equation (11), which is the result of omitting D from Equation (10).

$$\text{TOF}_{\text{bulk}} \left(\text{h}^{-1}\right) = \frac{\text{n} \cdot \text{X}}{\frac{\text{m}_{\text{Pd}}}{\text{M}_{\text{Pd}}} \cdot \text{t}} \quad (11)$$

For calculation of TOF_{bulk}, BnOH conversion at 1 h was utilized. The values of TOF_{bulk} are reported in Table S2.

4. Conclusions

In the search for new green nano-catalyst, Pd-P alloy nanoparticles were supported on the high-surface area silica functionalized by 3-APTES, and the product was compared with the corresponding Pd°/NH_2-SiO_2 catalyst. The XRD, BET, SEM, TEM characterizations of the two catalysts evidenced that they consisted of amorphous silica particles functionalized by aminopropyl groups with meso-pores of very similar dimensions, with nearly spherical Pd° or Pd-P NPs homogenously distributed on the surface. XRD and XPS characterization revealed that on the Pd-P/NH_2-SiO_2, the palladium was loaded as a Pd-phosphide alloy with a stoichiometric excess, being the atomic ratio Pd/P = 2. Palladium NPs were smaller in the Pd-P/NH_2-SiO_2 sample, suggesting that the formation of the Pd-P alloy favours the metal dispersion.

Pd-P/NH_2-SiO_2 was active for the oxidation of BnOH to PhCHO, and its activity was significantly influenced by the nature of the solvent, whereas Pd°/NH_2-SiO_2 was almost inactive regardless of the solvent. The better catalytic activity of Pd-P alloy might be explained by the lower electron density on Pd due to the presence of phosphorous and/or by the smaller particle size of Pd-P alloy. The best performance of Pd-P/NH_2-SiO_2 occurred in the non-polar non-protic toluene. In this solvent, the BnOH conversion and the TOF increased significantly by the temperature up to boiling point. Using pure O_2 instead of air as oxidant caused a further increase in the conversion from 57 to 78%. The best selectivity was obtained at 80 °C; nevertheless, the PhCHO yield increased by the temperature up to the boiling point, due to the significant increase of the conversion. The highest TOF of Pd-P/NH_2-SiO_2 (5982 h^{-1}) was achieved at the boiling point of toluene and in the presence of pure oxygen.

Supplementary Materials: The following are available online at https://www.mdpi.com/article/10.3390/catal12010020/s1, Figure S1: Materials produced by loading (**a**) Pd° and (**b**) Pd-P alloy particles on pristine silica support; Figure S2: Products of palladium nanoparticles syntheses, varying the Oam/TOP ratio and the reaction time; Figure S3: (**a**) Pd°/NH_2-SiO_2 and (**b**) Pd-P/NH_2-SiO_2 before final drying. Table S1: Effect of 3-APTES concentration on surface area of SiO_2 nanoparticles. Figure S4: Recyclability of Pd-P/NH_2-SiO_2 in terms of PhCHO yield. Table S2: Details of calculation of TOF and TOFbulk of Pd-P/NH_2-SiO_2.

Author Contributions: Conceptualization, I.L., S.S.M.; investigation and formal analysis, S.S.M., E.M., I.L., S.T., U.P.L.; SEM analysis, E.S.; XPS analysis, N.L. and R.C.; resources, I.L., S.T., D.T.; data curation, S.S.M., S.T., U.P.L., I.L., D.T.; writing—original draft preparation, S.S.M., S.T.; writing—review and editing, S.S.M., S.T., D.T., U.P.L., I.L. All authors have read and agreed to the published version of the manuscript.

Funding: This research was supported by grants from Ministero dell'Istruzione dell'Università e della Ricerca (MIUR)—Departments of Excellence, 2017—legge 232/2016—art.1, commi 314–337 awarded to Dept. of Science, University Roma Tre, Rome, Italy for 2018–2022.

Data Availability Statement: The data presented in this study are available on request from the corresponding author.

Acknowledgments: The authors greatly appreciate the helpful contribution of Sergio Lo Mastro, Dep. of Science, Università Roma Tre, for performing the XRD analysis.

Conflicts of Interest: The authors declare no conflict of interest.

References

1. Davis, S.E.; Ide, M.S.; Davis, R.J. Selective Oxidation of Alcohols and Aldehydes over Supported Metal Nanoparticles. *Green Chem.* **2013**, *15*, 17–45. [CrossRef]
2. Olenin, A.Y.; Mingalev, P.G.; Lisichkin, G.V. Partial Catalytic Oxidation of Alcohols: Catalysts Based on Metals and Metal Coordination Compounds (a Review). *Pet. Chem.* **2018**, *58*, 577–592. [CrossRef]
3. Giang, L.T.K.; Ku, Y. Selective Oxidation of Benzyl Alcohol in Aqueous Phase by TiO_2 Based Photocatalysts: A Review. *Chem. Eng. Technol.* **2021**, *14*, 2178–2190. [CrossRef]
4. Wu, P.; Song, L.; Wang, Y.; Liu, X.; He, Z.; Bai, P.; Yan, Z. High-Performance Benzyl Alcohol Oxidation Catalyst: Au-Pd Alloy with ZrO_2 as Promoter. *Appl. Surf. Sci.* **2021**, *537*, 148059. [CrossRef]
5. Choudhary, V.R.; Chaudhari, P.A.; Narkhede, V.S. Solvent-Free Liquid Phase Oxidation of Benzyl Alcohol to Benzaldehyde by Molecular Oxygen Using Non-Noble Transition Metal Containing Hydrotalcite-like Solid Catalysts. *Catal. Commun.* **2003**, *4*, 171–175. [CrossRef]
6. Marotta, R.; Di Somma, I.; Spasiano, D.; Andreozzi, R.; Caprio, V. Selective Oxidation of Benzyl Alcohol to Benzaldehyde in Water by TiO_2/Cu(II)/UV Solar System. *Chem. Eng. J.* **2011**, *172*, 243–249. [CrossRef]
7. Ahmad, N.; Alam, M.; Adil, S.F.; Ansari, A.A.; Assal, M.E.; Ramay, S.M.; Ahmed, M.; Alam, M.M.; Siddiqui, M.R.H. Synthesis, Characterization, and Selective Benzyl Alcohol Aerobic Oxidation over Ni-Loaded $BaFeO_3$ Mesoporous Catalyst. *J. King Saud Univ. Sci.* **2020**, *32*, 2059–2068. [CrossRef]
8. Kunene, A.; Leteba, G.; van Steen, E. Liquid Phase Oxidation of Benzyl Alcohol over Pt and Pt–Ni Alloy Supported on TiO_2: Using O_2 or H_2O_2 as Oxidant? *Catal. Lett.* **2021**, *2021*, 1–9. [CrossRef]
9. Moeini, S.S.; Battocchio, C.; Casciardi, S.; Luisetto, I.; Lupattelli, P.; Tofani, D.; Tuti, S. Oxidized Palladium Supported on Ceria Nanorods for Catalytic Aerobic Oxidation of Benzyl Alcohol to Benzaldehyde in Protic Solvents. *Catalysts* **2019**, *9*, 847. [CrossRef]
10. Guo, W.; Niu, S.; Shi, W.; Zhang, B.; Yu, W.; Xie, Y.; Ji, X.; Wu, Y.; Su, D.; Shao, L. Pd–P Nanoalloys Supported on a Porous Carbon Frame as an Efficient Catalyst for Benzyl Alcohol Oxidation. *Catal. Sci. Technol.* **2018**, *8*, 2333–2339. [CrossRef]
11. Xin, P.; Li, J.; Xiong, Y.; Wu, X.; Dong, J.; Chen, W.; Wang, Y.; Gu, L.; Luo, J.; Rong, H.; et al. Revealing the Active Species for Aerobic Alcohol Oxidation by Using Uniform Supported Palladium Catalysts. *Angew. Chem.* **2018**, *130*, 4732–4736. [CrossRef]
12. Chen, Y.; Guo, Z.; Chen, T.; Yang, Y. Surface-Functionalized TUD-1 Mesoporous Molecular Sieve Supported Palladium for Solvent-Free Aerobic Oxidation of Benzyl Alcohol. *J. Catal.* **2010**, *275*, 11–24. [CrossRef]
13. Alshammari, H.M. Synthesis of Palladium and Copper Nanoparticles Supported on TiO_2 for Oxidation Solvent-Free Aerobic Oxidation of Benzyl Alcohol. *Processes* **2021**, *9*, 1590. [CrossRef]
14. Yi, X.-T.; Zhao, T.; Wang, F.; Xu, J.; Xue, B. Palladium Nanoparticles Supported on Exfoliated G-C_3N_4 as Efficient Catalysts for Selective Oxidation of Benzyl Alcohol by Molecular Oxygen. *New J. Chem.* **2021**, *45*, 13519–13528. [CrossRef]
15. Savara, A.; Chan-Thaw, C.E.; Rossetti, I.; Villa, A.; Prati, L. Benzyl Alcohol Oxidation on Carbon-Supported Pd Nanoparticles: Elucidating the Reaction Mechanism. *ChemCatChem* **2014**, *6*, 3464–3473. [CrossRef]

16. Sabaté, F.; Jordà, J.L.; Sabater, M.J. Ruthenium Isomorphic Substitution into Manganese Oxide Octahedral Molecular Sieve OMS-2: Comparative Physic-Chemical and Catalytic Studies of Ru versus Abundant Metal Cationic Dopants. *Catal. Today* **2021**, in press. [CrossRef]
17. Mahdavi-Shakib, A.; Sempel, J.; Hoffman, M.; Oza, A.; Bennett, E.; Owen, J.S.; Rahmani Chokanlu, A.; Frederick, B.G.; Austin, R.N. Au/TiO_2-Catalyzed Benzyl Alcohol Oxidation on Morphologically Precise Anatase Nanoparticles. *ACS Appl. Mater. Interfaces* **2021**, *13*, 11793–11804. [CrossRef] [PubMed]
18. Chan-Thaw, C.E.; Savara, A.; Villa, A. Selective Benzyl Alcohol Oxidation over Pd Catalysts. *Catalysts* **2018**, *8*, 431. [CrossRef]
19. Villa, A.; Plebani, M.; Schiavoni, M.; Milone, C.; Piperopoulos, E.; Galvagno, S.; Prati, L. Tuning Hydrophilic Properties of Carbon Nanotubes: A Challenge for Enhancing Selectivity in Pd Catalyzed Alcohol Oxidation. *Catal. Today* **2012**, *186*, 76–82. [CrossRef]
20. Villa, A.; Schiavoni, M.; Prati, L. Material Science for the Support Design: A Powerful Challenge for Catalysis. *Catal. Sci. Technol.* **2012**, *2*, 673–682. [CrossRef]
21. Long, R.; Huang, H.; Li, Y.; Song, L.; Xiong, Y. Palladium-Based Nanomaterials: A Platform to Produce Reactive Oxygen Species for Catalyzing Oxidation Reactions. *Adv. Mater.* **2015**, *27*, 7025–7042. [CrossRef] [PubMed]
22. Wang, S.; Zhang, M.; Zhong, L.; Zhang, W. A Strategy to Immobilize Noble Metal Nanoparticles on Silica Microspheres. *J. Mol. Catal. A Chem.* **2010**, *327*, 92–100. [CrossRef]
23. Fedorenko, S.; Jilkin, M.; Nastapova, N.; Yanilkin, V.; Bochkova, O.; Buriliov, V.; Nizameev, I.; Nasretdinova, G.; Kadirov, M.; Mustafina, A.; et al. Surface Decoration of Silica Nanoparticles by Pd(0) Deposition for Catalytic Application in Aqueous Solutions. *Colloids Surf. A Physicochem. Eng. Asp.* **2015**, *486*, 185–191. [CrossRef]
24. Terra, J.C.S.; Moores, A.; Moura, F.C.C. Amine-Functionalized Mesoporous Silica as a Support for on-Demand Release of Copper in the A3-Coupling Reaction: Ultralow Concentration Catalysis and Confinement Effect. *ACS Sustain. Chem. Eng.* **2019**, *7*, 8696–8705. [CrossRef]
25. Fihri, A.; Cha, D.; Bouhrara, M.; Almana, N.; Polshettiwar, V. Fibrous Nano-Silica (KCC-1)-Supported Palladium Catalyst: Suzuki Coupling Reactions Under Sustainable Conditions. *ChemSusChem* **2012**, *5*, 85–89. [CrossRef]
26. Sadeghzadeh, S.M.; Zhiani, R.; Emrani, S. Pd/APTPOSS@KCC-1 as a New and Efficient Support Catalyst for C–H Activation. *RSC Adv.* **2017**, *7*, 24885–24894. [CrossRef]
27. Li, Y.; Sabbaghi, A.; Huang, J.; Li, K.C.; Tsui, L.S.; Lam, F.L.Y.; Hu, X. Aerobic Oxidation of Benzyl Alcohol: Influence from Catalysts Basicity, Acidity, and Preparation Methods. *Mol. Catal.* **2020**, *485*, 110789. [CrossRef]
28. Opanasenko, M.; Štěpnička, P.; Čejka, J. Heterogeneous Pd Catalysts Supported on Silica Matrices. *RSC Adv.* **2014**, *4*, 65137–65162. [CrossRef]
29. Chen, Y.; Lim, H.; Tang, Q.; Gao, Y.; Sun, T.; Yan, Q.; Yang, Y. Solvent-Free Aerobic Oxidation of Benzyl Alcohol over Pd Monometallic and Au–Pd Bimetallic Catalysts Supported on SBA-16 Mesoporous Molecular Sieves. *Appl. Catal. A Gen.* **2010**, *380*, 55–65. [CrossRef]
30. Zhang, K.; Wang, C.; Bin, D.; Wang, J.; Yan, B.; Shiraishi, Y.; Du, Y. Fabrication of Pd/P Nanoparticle Networks with High Activity for Methanol Oxidation. *Catal. Sci. Technol.* **2016**, *6*, 6441–6447. [CrossRef]
31. Su, W.; Sun, R.; Ren, F.; Yao, Y.; Fei, Z.; Wang, H.; Liu, Z.; Xing, R.; Du, Y. Graphene Supported Palladium-Phosphorus Nanoparticles as a Promising Catalyst for Ethylene Glycol Oxidation. *Appl. Surf. Sci.* **2019**, *491*, 735–741. [CrossRef]
32. Yang, Z.; Klabunde, K.J. Synthesis of Nearly Monodisperse Palladium (Pd) Nanoparticles by Using Oleylamine and Trioctylphosphine Mixed Ligands. *J. Organomet. Chem.* **2009**, *694*, 1016–1021. [CrossRef]
33. Yoshida, R.; Sun, D.; Yamada, Y.; Sato, S. Stable Cu-Ni/SiO_2 Catalysts Prepared by Using Citric Acid-Assisted Impregnation for Vapor-Phase Hydrogenation of Levulinic Acid. *Mol. Catal.* **2018**, *454*, 70–76. [CrossRef]
34. Chen, Y. Chemical Preparation and Characterization of Metal–Metalloid Ultrafine Amorphous Alloy Particles. *Catal. Today* **1998**, *44*, 3–16. [CrossRef]
35. Yang, C.; Zhang, J.; Han, S.; Wang, X.; Wang, L.; Yu, W.; Wang, Z. Compositional Controls on Pore-Size Distribution by Nitrogen Adsorption Technique in the Lower Permian Shanxi Shales, Ordos Basin. *J. Nat. Gas Sci. Eng.* **2016**, *34*, 1369–1381. [CrossRef]
36. Thommes, M.; Kaneko, K.; Neimark, A.V.; Olivier, J.P.; Rodriguez-Reinoso, F.; Rouquerol, J.; Sing, K.S.W. Physisorption of Gases, with Special Reference to the Evaluation of Surface Area and Pore Size Distribution (IUPAC Technical Report). *Pure Appl. Chem.* **2015**, *87*, 1051–1069. [CrossRef]
37. Abbas, S.H.; Adam, F.; Muniandy, L. Green Synthesis of MCM-41 from Rice Husk and Its Functionalization with Nickel(II) Salen Complex for the Rapid Catalytic Oxidation of Benzyl Alcohol. *Microporous Mesoporous Mater.* **2020**, *305*, 110192. [CrossRef]
38. Chandra, S.; Beaune, G.; Shirahata, N.; Winnik, F.M. A One-Pot Synthesis of Water Soluble Highly Fluorescent Silica Nanoparticles. *J. Mater. Chem. B* **2017**, *5*, 1363–1370. [CrossRef]
39. Liu, Y.; McCue, A.J.; Miao, C.; Feng, J.; Li, D.; Anderson, J.A. Palladium Phosphide Nanoparticles as Highly Selective Catalysts for the Selective Hydrogenation of Acetylene. *J. Catal.* **2018**, *364*, 406–414. [CrossRef]
40. Lu, C.; Wang, M.; Feng, Z.; Qi, Y.; Feng, F.; Ma, L.; Zhang, Q.; Li, X. A Phosphorus–Carbon Framework over Activated Carbon Supported Palladium Nanoparticles for the Chemoselective Hydrogenation of Para-Chloronitrobenzene. *Catal. Sci. Technol.* **2017**, *7*, 1581–1589. [CrossRef]
41. Belykh, L.B.; Skripov, N.I.; Sterenchuk, T.P.; Akimov, V.V.; Tauson, V.L.; Savanovich, T.A.; Schmidt, F.K. Role of Phosphorus in the Formation of Selective Palladium Catalysts for Hydrogenation of Alkylanthraquinones. *Appl. Catal. A Gen.* **2020**, *589*, 117293. [CrossRef]

42. Wu, K.; Mao, X.; Liang, Y.; Chen, Y.; Tang, Y.; Zhou, Y.; Lin, J.; Ma, C.; Lu, T. Multiwalled Carbon Nanotubes Supported Palladium–Phosphorus Nanoparticles for Ethanol Electrooxidation in Alkaline Solution. *J. Power Sources* **2012**, *219*, 258–262. [CrossRef]
43. Rego, R.; Ferraria, A.M.; Botelho do Rego, A.M.; Oliveira, M.C. Development of PdP Nano Electrocatalysts for Oxygen Reduction Reaction. *Electrochim. Acta* **2013**, *87*, 73–81. [CrossRef]
44. Lv, H.; Sun, L.; Xu, D.; Ma, Y.; Liu, B. When Ternary PdCuP Alloys Meet Ultrathin Nanowires: Synergic Boosting of Catalytic Performance in Ethanol Electrooxidation. *Appl. Catal. B Environ.* **2019**, *253*, 271–277. [CrossRef]
45. Okamoto, H. The P-Pd (Phosphorus-Palladium) System. *JPE* **1994**, *15*, 58–61. [CrossRef]
46. Kucernak, A.R.J.; Fahy, K.F.; Sundaram, V.N.N. Facile Synthesis of Palladium Phosphide Electrocatalysts and Their Activity for the Hydrogen Oxidation, Hydrogen Evolutions, Oxygen Reduction and Formic Acid Oxidation Reactions. *Catal. Today* **2016**, *262*, 48–56. [CrossRef]
47. Chen, J.; Zhang, Q.; Wang, Y.; Wan, H. Size-Dependent Catalytic Activity of Supported Palladium Nanoparticles for Aerobic Oxidation of Alcohols. *Adv. Synth. Catal.* **2008**, *350*, 453–464. [CrossRef]
48. Savara, A.; Rossetti, I.; Chan-Thaw, C.E.; Prati, L.; Villa, A. Microkinetic Modeling of Benzyl Alcohol Oxidation on Carbon-Supported Palladium Nanoparticles. *ChemCatChem* **2016**, *8*, 2482–2491. [CrossRef]
49. Savara, A.; Chan-Thaw, C.E.; Sutton, J.E.; Wang, D.; Prati, L.; Villa, A. Molecular Origin of the Selectivity Differences between Palladium and Gold–Palladium in Benzyl Alcohol Oxidation: Different Oxygen Adsorption Properties. *ChemCatChem* **2017**, *9*, 253–257. [CrossRef]
50. Wang, J.; Teschner, D.; Huang, X.; Yao, Y.; Willinger, M.; Shao, L.; Schlögl, R. Nanosized Palladium on Holey Graphene Sheets Incorporating P_xO_y for Effective Formic Acid Oxidation. *Electrochem. Commun.* **2017**, *74*, 24–27. [CrossRef]
51. Sahu, D.; Sarmah, C.; Das, P. A Highly Efficient and Recyclable Silica-Supported Palladium Catalyst for Alcohol Oxidation Reaction. *Tetrahedron Lett.* **2014**, *55*, 3422–3425. [CrossRef]
52. Li, A.; Tang, S.; Tan, P.; Liu, C.; Liang, B. Measurement and Prediction of Oxygen Solubility in Toluene at Temperatures from 298.45 K to 393.15 K and Pressures up to 1.0 MPa. *J. Chem. Eng. Data* **2007**, *52*, 2339–2344. [CrossRef]
53. Horstmann, S.; Grybat, A.; Kato, R. Experimental Determination and Prediction of Gas Solubility Data for Oxygen in Acetonitrile. *J. Chem. Thermodyn.* **2004**, *36*, 1015–1018. [CrossRef]
54. Yang, Z.-W.; Zhao, X.; Li, T.-J.; Chen, W.-L.; Kang, Q.-X.; Xu, X.-Q.; Liang, X.-X.; Feng, Y.; Duan, H.-H.; Lei, Z. Catalytic Properties of Palygorskite Supported Ru and Pd for Efficient Oxidation of Alcohols. *Catal. Commun.* **2015**, *65*, 34–40. [CrossRef]
55. Galvanin, F.; Sankar, M.; Cattaneo, S.; Bethell, D.; Dua, V.; Hutchings, G.J.; Gavriilidis, A. On the Development of Kinetic Models for Solvent-Free Benzyl Alcohol Oxidation over a Gold-Palladium Catalyst. *Chem. Eng. J.* **2018**, *342*, 196–210. [CrossRef]
56. Bergeret, G.; Gallezot, P. Particle Size and Dispersion Measurements. In *Handbook of Heterogeneous Catalysis*; American Cancer Society: Atlanta, GA, USA, 2008; pp. 738–765, ISBN 978-3-527-61004-4.
57. Moulder, J.F.; Stickle, W.F.; Sobol, P.E.; Bomben, K.D. *Handbook of X-ray Photoelectron Spectroscopy: A Reference Book of Standard Spectra for Identification and Interpretation of XPS Data*; Chastain, J., King, R.C., Jr., Eds.; Physical Electronics Division, Perkin-Elmer Corporation: Eden Prairie, MN, USA, 1992; ISBN 978-0-9627026-2-4.